PCCP

Accepted Manuscript

ROYAL SOCIETY OF CHEMISTRY

www.rsc.org/pccp

PCCP

PAPER

Excited-State Dynamics of Si-Rhodamine and Its Aggregates: Versatile Fluorophore for NIR Absorption†

Received 00th January 20xx,
Accepted 00th January 20xx

DOI: 10.1039/x0xx00000x

www.rsc.org/

Sooyeon Kim, Mamoru Fujitsuka, Mikiji Miyata, Tetsuro Majima*

Since it was first reported in 2008, great attention has been paid to Si-rhodamine (SiR) because of its far-red to near-infrared (NIR) absorption/fluorescence and suitability for high-resolution *in vivo* imaging. However, properties of SiR in the excited state have not been reported, even though they are directly related to its fluorescence. In the present study, the properties of SiR monomer in the excited states are thoroughly characterized for the first time. Moreover, by replacing a phenyl moiety of SiR with a 4-(9-anthryl)phenylene group (**SiR-An**), we prepared H- and J-aggregate of SiR in the aqueous solution, and succeeded in monitoring exciton formation and annihilation in the aggregates. Interestingly, the relative exciton population in SiR J-aggregate increases as the excitation power becomes stronger, which is unusual concerning that the substantial exciton-exciton annihilation process occurs as more excitons are generated. The obtained results in the present study suggest high versatility of SiR not only as a red fluorophore in the cutting-edge microscopic techniques but also as a NIR absorber in the light harvesting system.

1. Introduction

Si-rhodamine (SiR) is a family of far-red fluorescent rhodamine derivatives that replace the oxygen with a silicon atom in the typical rhodamine dyes such as tetramethylrhodamine (TMR) (Fig. 1). This interesting attempt was firstly made by Fu et al. in 2008 in order to introduce extremely low level of lowest unoccupied molecular orbital (LUMO) and rapid electron mobility that many silico-cyclic aromatic compounds exhibit.[1] Although silylation is a common approach in the material development such as luminescent materials, it brings about new paradigm in fluorescence microscopy for living matters since Koide et al. presented group 14 rhodamine series for biological imaging in 2011.[2]

One of the important properties of SiR as a fluorophore is its far-red to near-infrared (NIR) absorption and fluorescence due to the low LUMO level of a silicon atom.[1, 2] Meanwhile, it still keeps properties of original rhodamine dyes such as high fluorescence quantum yield (Φ_{fl} = 0.3–0.45) and cell permeability.[2] In this decade, technology of fluorescence microscopy has incredibly proceeded, and monitoring fluorescence of a single fluorophore or visualizing extremely small intracellular target within a few tens nm have become possible.[3, 4] Since living matters intrinsically possess endogenous chromophores resulting in autofluorescence,[5, 6] fluorophores which are excited by far-red to NIR photoirradiation are highly required for cutting-edge microscopic techniques. In this sense, SiR has received substantial attention and there have been great improvement in fluorescence imaging with the aid of SiR.[9-12] Fluorescence is one of the relaxation pathways and closely related to the properties of SiR in the excited state, but it is surprising that there have been no photophysical study about SiR.

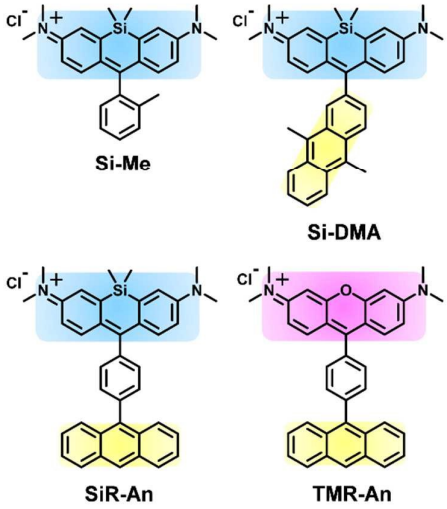

Fig. 1 Chemical structures of SiR and TMR derivatives used in the present study. Blue, yellow, and pink boxes represent chromophore parts of SiR, anthracene, and TMR derivatives, respectively. Preparation of the compounds can be found in the previous reports.[7, 8]

The Institute of Scientific and Industrial Research (SANKEN), Osaka University, Mihogaoka 8-1, Ibaraki, Osaka 567-0047 (Japan)

† Electronic supplementary information (ESI) available. See DOI: 10.1039/x0xx00000x

In addition, the absorption and fluorescence spectra of TMR-originated SiR are limited to far-red region ($\lambda_{abs,\ max}$ and $\lambda_{fl,\ max}$ in methanol are about 650 and 670 nm, respectively). To widen the usage of SiR from a red fluorophore to NIR absorber in the light harvesting system, absorption spectrum of SiR requires a further red shift to absorb light in the NIR region (> 700 nm). In this aspect, we focus on the aggregation behavior of fluorophore, which often provides unexpected and interesting properties, such as an abrupt increase in fluorescence or spectral changes in color and fluorescence.[13-17] Very recently, we have reported that replacing a phenyl group with a 4-(9-anthryl)phenylene group in rhodamine dyes can lead to the formation of a slipped-stacked self-assembly of TMR and SiR (**TMR-An** and **SiR-An**, respectively) without a help of additional templates.[7] In the presence of halide ion, **SiR-An** can undergo a spontaneous transition of the assembly pattern from parallel-stacked (H-aggregate) to slipped-stacked assemblies (J-aggregate, Fig. S1). The conversion between H- and J-aggregates is accompanied by a discoloration of a J-aggregate of **SiR-An** originating from a dramatic red shift of absorption maxima from 650 to 745 nm (Fig. S3a). X-ray crystallographic analysis indicated that rhodamine and anthracene moieties may initially form head-to-tail dimers, and π-electrons of the C-N bond at both ends of the rhodamine moieties subsequently stabilize slipped–stacked rhodamine–rhodamine arrays (Fig. S3c).[7]

The above systems exhibit several fascinating aspects worthy of further photophysical studies. First, through introducing a 4-(9-anthryl)phenylene group, we could prepare a well–aligned slipped–stacked rhodamine J-aggregate. This indicates that we can study and compare the dynamics of exciton generated in several types of rhodamine self-assemblies, which have not been prepared before without the help of external templates. Second, the rhodamine J-aggregate showed decreased fluorescence compared with that of the monomer (Fig. S3b), whereas most J-aggregates are fluorescent because the lower exciton level of J-coupling is spin-allowed and can undergo radiative relaxation. To explain this anomaly, the excited-state dynamics of these systems should be investigated further.

Indeed, self-assembly formation and the dynamics of charge and energy transport through the building blocks are of central importance in the development of photovoltaics, optoelectronic devices, and solar cells.[18, 19] In nature, the characteristic slipped–stacked alignments of chlorophylls and bacteriochlorophylls form efficient light-harvesting systems for photosynthesis. If intermolecular and non-covalent interactions between chlorophylls are disrupted, the dense self-assembly will be affected and ultrafast energy transfer to the reaction center will no longer be achieved. As well as in regards to nanodevice development, the formation of chromophore aggregates is also an intriguing phenomenon for the design of fluorescence probes based on properties such as aggregation-induced emission and colorimetric changes.[13-16, 20-22]

In the present study, using the femtosecond laser flash photolysis (fs-LFP), nanosecond laser flash photolysis (ns-LFP), and pulse radiolysis, we thoroughly examined the excited-state dynamics of a SiR monomer, H- and J-aggregate. As a result, extinction coefficients

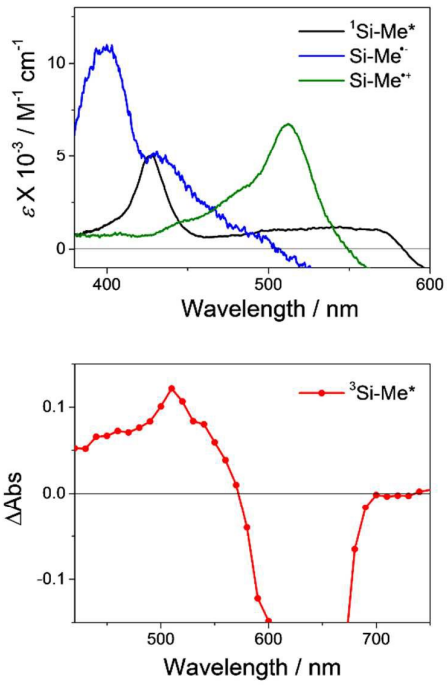

Fig. 2 (a) Transient absorption spectra of ^{1}**Si-Me*** (black) in methanol observed at 3 ps after an excitation pulse measured during the fs-LFP, and **Si-Me**$^{\bullet-}$ (blue) and **Si-Me**$^{\bullet+}$ (green) in the deaerated aqueous solutions measured at 5 μs after an excitation during the pulse radiolysis. (b) ^{3}**Si-Me*** in deaerated methanol measured at 20 ps after an excitation during the ns-LFP in the presence of triplet energy donor, anthracene ([**Si-Me**] = 100 μM, [anthracene] = 300 μM), λ_{ex} = 355 nm at 5 mJ pulse^{-1}. The detailed conditions of the spectroscopic measurements are described in the ESI.

Table 1 ε of **Si-Me** in the excited state and radical ions of **Si-Me**.

Species	λ_{max} / nm	ε / M^{-1} cm^{-1}	Solvent	Method
^{1}**Si-Me***	427	5,000	Methanol	fs-LFP
^{3}**Si-Me***	510	n.d.†	Methanol	ns-LFP
Si-Me$^{\bullet-}$	399	10,900	PBS	Pulse radiolysis
Si-Me$^{\bullet+}$	512	6,760	MilliQ	Pulse radiolysis

†n.d.: Not determined.

(ε) of various transient species of SiR were determined, and exciton formation and annihilation in H- and J-aggregates of **SiR-An** were successfully monitored. This article is the first report on the SiR photophysics and direct monitoring of the exciton generated in SiR J-aggregates. Moreover, increased exciton population in SiR J-aggregate under the stronger excitation condition suggests a prospective usage of SiR as a NIR absorber in the light harvesting system that demands long exciton lifetime rather than a rapid annihilation process.

2. Results and Discussion

2.1. Transient absorption spectra of Si-Me in the excited state

As mentioned above, SiR has recently received considerable attentions because of their far-red to NIR absorption/fluorescence, good cell-permeability dependent on the chemical modification, and suitability for superresolution fluorescence microscopy.[9-12] Most of the studies are exploiting emission property of SiR, which implies the urgent requirement of study on SiR in the excited state. Herein, owing to study the property of SiR monomer, we prepared **Si-Me** (Fig. 1) which is moderately water-soluble.

First of all, transient absorption spectra of **Si-Me** in the singlet excited state (^{1}**Si-Me***, Fig. S4), the triplet excited state (^{3}**Si-Me***), **Si-Me**$^{\bullet-}$, and **Si-Me**$^{\bullet+}$ were measured by the fs-LFP, ns-LFP, and pulse radiolysis of the **Si-Me** monomer, respectively. As shown in Fig. 2, all of the transient spectra resemble those of previously reported rhodamine derivatives, such as rhodamine 123, with a red shift of 20–80 nm.[23] The ε of **Si-Me** in the excited state are summarized in Table 1. Since **Si-Me** represents a monomeric SiR, we denoted the chromophore part of **Si-Me** (blue boxes in Fig. 1) as SiR from the next chapter to avoid confusion.

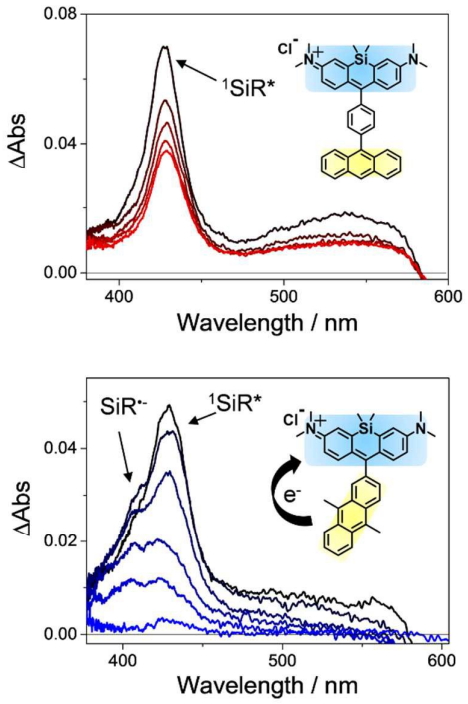

Fig. 3 (a) Transient absorption spectra monitored at 0.4, 5.2, 17, 53, and 73 ps (black to red) after a laser pulse during the fs-LFP of the **SiR-An** monomer in methanol excited at 650 nm. (b) Transient absorption spectra monitored at 0.4, 1.2, 3.0, 5.2, 10.2, and 53 ps (black to blue) after a laser pulse during the fs-LFP of **Si-DMA** monomer in methanol excited at 650 nm.

2.2. Properties of SiR-An in the ground state and singlet excited state

SiR-An is the derivative of SiR (Fig. 1) that we recently designed for the self-assembly formation in the aqueous solution.[7] **SiR-An** exhibits far-red absorption and fluorescence with maxima at λ_{abs} = 648 nm and λ_{fl} = 667 nm in methanol, respectively, similar to other SiR derivatives.[7] However, Φ_{fl} and τ_{fl} of **SiR-An** were 0.05 and 0.75 ns in methanol, respectively (Table S1), which are 6-fold weaker and five times shorter, respectively, than the same properties of SiR without an anthracene moiety, **Si-Me**.[7] A similar phenomenon was observed for hydroxyphenylfluorone, a dyad of fluorescein and benzene, which displayed a Φ_{fl} four times smaller than that of Tokyo Green, which is a dyad of fluorescein and 2-methylbenzene.[24] This is because methyl substitution at the 2-position of the benzene prohibits rotation between fluorescein and phenyl moieties in Tokyo Green, whereas this geometric hindrance does not exist in hydroxyphenylfluorone, resulting in an increased rate of internal conversion. Therefore, if there is no faster additional relaxation process apart from fluorescence, the weaker fluorescence of **SiR-An** than **Si-Me** originates from the increased rate of internal conversion, caused by increased freedom of the ring rotation between SiR and phenylene moieties. Another plausible quenching process is photoinduced electron transfer (PET) that occurs from the anthracene moiety to SiR moiety in the excited state, resulting in a charge-separated state.

To confirm the occurrence of PET in **SiR-An**, one should perform transient absorption measurements to determine whether or not charge-separated states are formed. In consequence, as illustrated in Fig. 3a, transient absorption spectra of **SiR-An** in the shorter wavelength region closely resemble that of ^{1}**Si-Me*** (black, Fig. 2a).

Meanwhile, radical species of **Si-Me** (blue and green, Fig. 2a) and the radical cation of anthracene (An$^{\bullet+}$)[25] were not observed in the transient absorption spectra of **SiR-An**. In addition, the LUMO and highest occupied molecular orbital (HOMO) of **SiR-An** are found to be located on the SiR moiety based on DFT calculation (Fig. S5), indicating the electron transfer will not occur among SiR and anthracene moieties. Taken together, the faster deactivation of ^{1}SiR* and weak fluorescence of **SiR-An** than those of **Si-Me** originates from an increased rate of internal conversion, not PET.

For comparison, we carried out the fs-LFP of **Si-DMA** (Fig. 1), a dyad of SiR and dimethylanthracene, which is deactivated by PET upon the selective excitation of SiR (Fig. 3b).[8] Although the signal from An$^{\bullet+}$ was obscured by overlap with considerable ground-state bleaching, SiR$^{\bullet-}$ was clearly detected and ^{1}SiR* decayed rapidly (within 50 ps). The Gibbs free energy for PET can be calculated by Rehm-Weller equation:[25, 26] $\Delta G_{PET} = (E_{ox}(D) - E_{red}(A)) - {}^1E_{00} - \Delta G_s$ where $E_{ox}(D)$, $E_{red}(A)$, $^1E_{00}$, and ΔG_s indicate the oxidation potential of the electron donor, reduction potential of the electron acceptor, singlet excited energy of SiR, and electrostatic work function, respectively. Using the reported values of the $E_{ox}(D)$ of dimethylanthracene and anthracene (1.05 and 1.19 V *vs*. SCE, respectively)[27] and $E_{red}(A)$ of SiR (–0.62 *vs*. SCE)[2] and the

experimental value of the $^1E_{00}$ of **Si-Me** (1.89 eV), the values for ($\Delta G_{PET} + \Delta G_s$) of **SiR-An** and **Si-DMA** are determined to be –0.08 and –0.22 eV, respectively. Even without the consideration of ΔG_s, which is usually small for the dyad that donor and acceptor moieties are directly connected each other,[26] **Si-DMA** has negative ΔG_{PET}, whereas **SiR-An** has near-zero to slight negative ΔG_{PET}. Considering the probable deviations in the reported values, the absence of charge-separated state in **SiR-An** is reasonable due to the higher E_{ox}(D) and smaller ΔG_s of **SiR-An** than those of **Si-DMA**.

As shown in Fig. S6b and S6c, **TMR-An** (Fig. 1) in the singlet excited state consequences in the same result to that of **SiR-An**. Based on the Rehm-Weller equation (the value of ($-E_{red}$(A) – $^1E_{00}$) for rhodamine B and calculated ($\Delta G_{PET} + \Delta G_s$) of **TMR-An** are –1.25 and –0.06 eV, respectively),[2] the prevention of PET is caused by the same reason to those of **SiR-An**.

2.3. Decay process of SiR-An H-aggregate in the excited state

In aqueous solution, SiR normally forms an H-aggregate in a similar manner to other rhodamine derivatives such as rhodamine B.[8, 9, 28] To study the dynamics of H-aggregate of **SiR-An** in the excited state, we could prepare it dissolved in the aqueous solution without the addition of NaCl (Fig. S3a). Based on the previous measurement of dynamic light scattering (DLS),[7] the size of **SiR-An** H-aggregate is smaller than a few nm, indicating this H-aggregate is composed of two or a few **SiR-An** monomers.

Fig. 4 reveals that the shapes of transient absorption spectra of SiR-An H-aggregates were considerably different from those of monomeric SiR-An. As for the SiR-An H-aggregate, mainly two transient species with τ = 0.6 and 16.8 ps that showed absorption maxima at 430 and 510 nm, respectively, were generated following 650-nm excitation (Fig. S7). It is notable that the deactivation mechanisms of H-aggregates depend on the characteristics of the chromophore. The most accepted deactivation mechanism for a rhodamine H-dimer is ultrafast internal conversion between two exciton bands on the sub-ps to ps-time scale, followed by intersystem crossing to form a dimer in the triplet excited state, because a direct transition from the lower exciton state to the ground state is forbidden in H-aggregates.[29, 30] Exciton trapping and excimer formation are also well-known relaxation pathways of H-aggregates.[31, 32] Because the transient absorption spectra of the H-aggregate resemble the superposition of various transient species of **Si-Me** (Fig. 2a), here, the transient species with τ = 0.6 and 16.8 ps were tentatively assigned to the exciton and 'intermediate' states, respectively (Fig. 7).

2.4. Dynamics and power dependence of exciton in SiR-An J-aggregate

As introduced earlier, **SiR-An** forms J-aggregates in the aqueous solution in the presence of halide ion.[7] The fluorescence of the **SiR-An** J-aggregate is negligible ($\lambda_{J,fl}$ = 746 nm, indicated by a red asterisk in Fig. S3b).[7] This is an unexpected phenomenon considering that a radiative relaxation process is allowed in J-aggregates, unlike in H-aggregates.[33, 34] Indeed, we observed an increase in the fluorescence intensity of monomer (λ_{fl} = 667 nm) upon endoperoxidation of the anthracene moiety of **SiR-An**, indicating the dissociation of J-aggregate induces fluorescence recovery (preliminary data, which will be published later). Here, the exciton dynamics formed in the **SiR-An** J-aggregate were directly monitored and investigated using the fs-LFP.

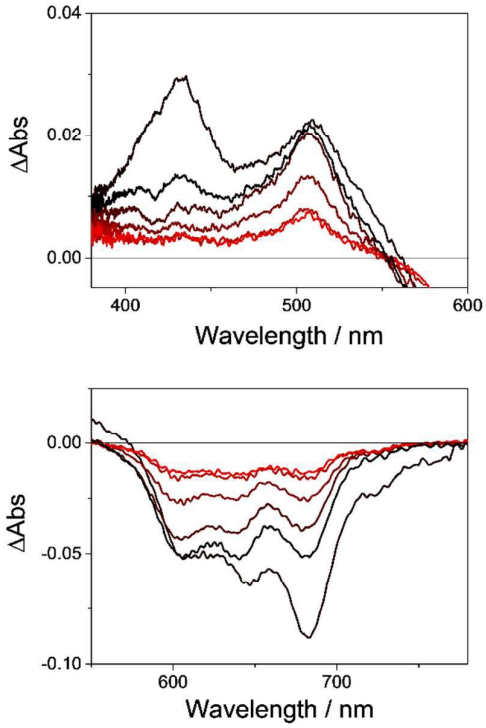

Fig. 4 Transient absorption spectra monitored at 0.4, 2.0, 5.2, 17, 53, and 73 ps (black to red) measured in the regions of (a) short (380-600 nm) and (b) long wavelengths (550-780 nm) after a laser pulse during the fs-LFP of the **SiR-An** H-aggregate in MilliQ water excited at 650 nm.

As shown in Fig. 5, negative transient absorption appearing at 730–750 nm and positive transient absorption appearing at shorter wavelengths than 730 nm were observed upon selective J-band excitation of **SiR-An** J-aggregate at 740 nm. The negative transient absorption at 730–750 nm reflects ground state bleaching of the **SiR-An** J-aggregate and a scattering signal induced by 740-nm excitation. The positive transient absorption appearing at shorter wavelengths than 730 nm is designated to the exciton formed in the **SiR-An** J-aggregate. Similar phenomena were observed for **TMR-An** J-aggregate (Fig. 6). Spectral shapes and decay profiles well resemble those of pseudoisocyanine J-aggregate,[35-37] which photophysics has been substantially studied for several decades.

Interestingly, the spectral shape and decay profile of the positive transient absorption were significantly affected by the excitation power (insets of Fig. 5). In the case of a high density of the excitation energy (15 μJ pulse^{-1}, Fig. 5a), the spectral shape of

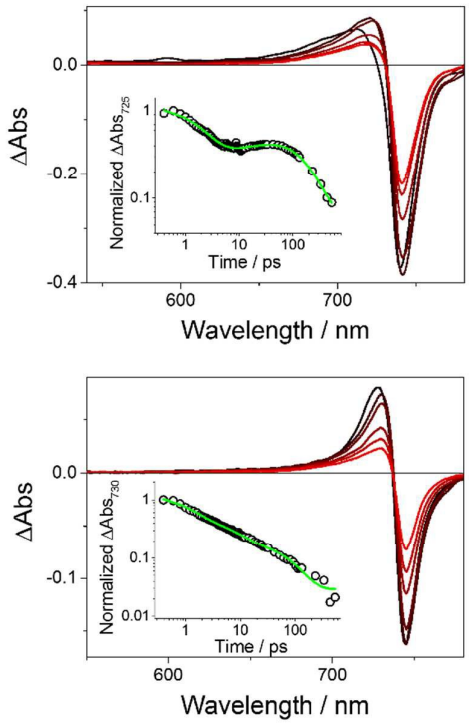

Fig. 5 Transient absorption spectra monitored at 0.4, 0.6, 0.8, 2.0, 5.0, and 10 ps (black to red) after a laser pulse during the fs-LFP of the **SiR-An** J-aggregates in the aqueous solution excited at 740 nm, near to the maximum of the J-band, at (a) 15 μJ pulse^{-1} and (b) 40 nJ pulse^{-1}. (inset) Time profile of positive transient absorption of **SiR-An** J-aggregates (open circles) and the fitting results (green line) using three-exponential function to guide the decay profile.

positive transient absorption is rather broad and shows 10-nm red-shift during the initial 1 ps. Similar phenomena has been reported previously for J-aggregate systems based on cyanine or porphyrin derivatives under strong excitation.[37-39] The short-lived state is assigned to be a two-exciton which is generated through the exciton-exciton annihilation (EEA) process (Fig. 7). This characteristic phenomena were more evident as excitation power increases (Fig. 5 and S8), which further supports that the spectral red-shift is due to the presence of higher excited states.

On the other hand, approximately 380 times smaller excitation intensity (40 nJ pulse^{-1}) induced a rapid decay of the exciton population within the initial 10 ps, but with less spectral change in a shape (Fig. 5b). In J-aggregate, it is expected that the EEA occurs, leading to the rapid reduction of the exciton population. However, we could not fit the time profile using the one- and three-dimensional EEA model (Fig. S10).[40-42] The previous reports pointed out that the deviation happens when aggregates are small and EEA is determined by the static rate of equilibrated excitons.[43, 44] DLS measurement of **SiR-An** J-aggregate revealed that there are two types of J-aggregate in a size, a few hundred nanometers and larger than a few micrometers.[7] Thus, the size of smaller aggregate was around 200–600 nm that probably contains more than 100 monomers based on the X-ray crystallographic data (Fig. S3c). However, the full width at half maximum of absorption band of **SiR-An** monomer and J-aggregate is approximately two-fold different (807 and 476 cm^{-1}, respectively), indicating the effective coherence length (N_{eff}) of **SiR-An** J-aggregate is much shorter in the aqueous solution (N_{eff} = $(\Delta\upsilon_{2/3}(M)/\Delta\upsilon_{2/3}(P))^2$ = 3.15 for **SiR-An** J-aggregate where $\Delta\upsilon_{2/3}(M)$ and $\Delta\upsilon_{2/3}(P)$ are the width at 2/3 maximum of the absorption band of monomer and J-aggregate, respectively)[43] than the ideally aligned nanocrystal. Taken together, it is reasonable that the standard model of EEA in film or crystal does not match well with **SiR-An** J-aggregate in the solution, which is caused by a probable presence of defects in the assembly.

As shown in Fig. 5a, the deviation from the standard EEA model becomes larger under the high excitation intensity. This is probably because of the generation of the additional state, which is long-lived (> 1 ns), followed by the EEA process (a rise shown at around 10 ps after a pulse in the inset of Fig. 5a). This result is opposite to the common characteristic of the EEA process; as excitation becomes stronger, the population of one-exciton decreases faster. Thus, we tentatively assume that the additionally generated species is a kind of the secondary-formed species such as vibrationally excited one-exciton state in addition to two-exciton state[37] or slipped-stacked excimer.[32, 45, 46] Complete assignment of this species generated under the strong excitation requires further investigations.

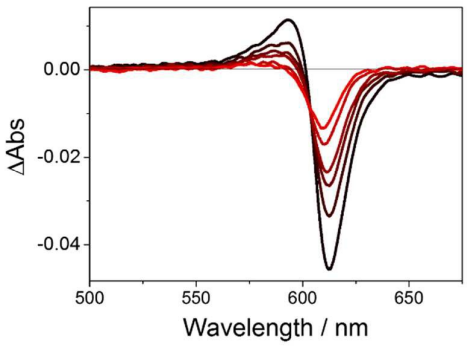

Fig. 6 Transient absorption spectra monitored at 0.4, 0.6, 0.8, 1.0, 2.0, and 5.0 ps (black to red) after a laser pulse during the fs-LFP of the **TMR-An** J-aggregates in the aqueous solution excited at 605 nm, near to the maximum of the J-band (2.0 μJ pulse^{-1}).

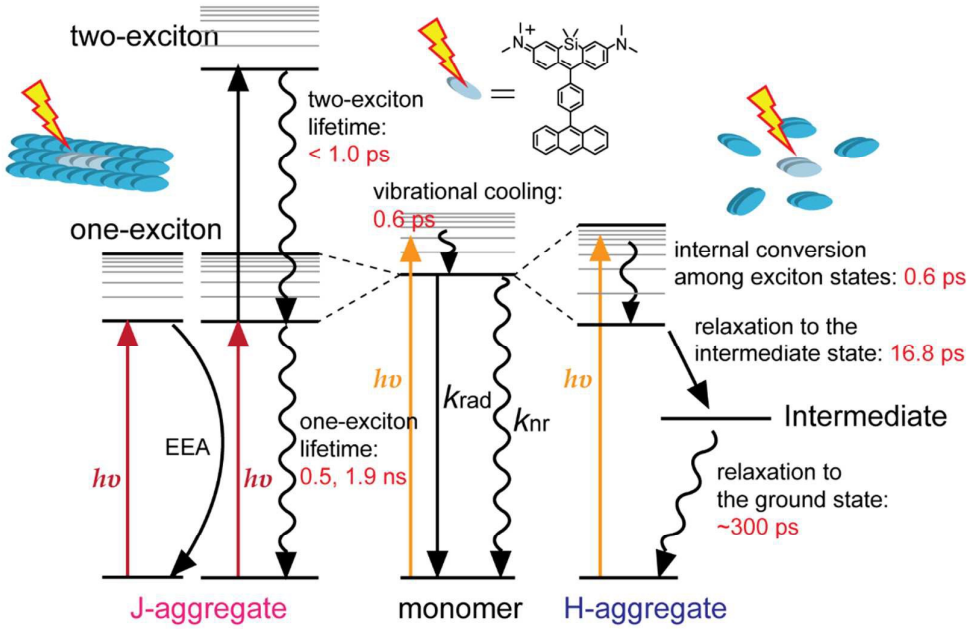

Fig. 7 Plausible relaxation pathways and time constants of the **SiR-An** monomer, H- and J-aggregate. Orange and red arrows indicate 650- and 740-nm excitations, respectively. The rates of radiative and non-radiative relaxation (k_{rad} and k_{nr}, respectively, as shown above) of **Si-Me** and **SiR-An** are summarized in Table S1. The intermediate state for H-aggregate relaxation may be either the triplet excited state or excimer state. In the case of J-aggregate, this pathway is only reasonable under the weak excitation power (40 nJ pulse^{-1}, Fig. 5b), because the strong excitation induces the formation of the additional species in the excited state (Fig. 5a). Two lifetimes of one-exciton state of **SiR-An** J-aggregate, 0.5 and 1.9 ns, were obtained by an exponential fitting of the decay profile in the range of 32–120 ps and 100–730 ps, respectively. We tentatively assume that the one-exciton lifetime strongly depends on the molecular alignment and excitation power.

Taken together, fluorescence quenching upon J-aggregate formation is considered to originate from efficient EEA even induced by the weak excitation power (40 nJ pulse^{-1}) and probable intermolecular interactions between SiR and anthracene moieties because of the decreased interchromophore distance upon J-aggregate formation.[47] As excitation intensity becomes stronger (> 0.3 nJ pulse^{-1}), however, a deviation from the standard EEA model becomes larger, indicating the formation of secondary species, which is long-lived. We believe this is an important finding since the strong excitation is often considered to cause a rapid reduction of exciton population through the efficient EEA process. The obtained results in the present study are summarized in Fig. 7. Furthermore, **TMR-An** monomer and its aggregate in the excited states seem to have similar properties (Fig. S6 and Fig. 6).

3. Conclusions

In the present study, we comprehensively investigated the excited-state dynamics of the SiR monomer, H- and J-aggregate for the first time using the fs-LFP, ns-LFP, and pulse radiolysis. As a result, we monitored the absorption spectra of various transient species of SiR and determined each ε. When SiR is substituted by anthracene derivatives, PET from anthracene to SiR in the singlet excited state occurred only when the anthracene derivative is directly connected to the chromophore of SiR (**Si-DMA**). If anthracene and SiR is separated by a phenylene group (**SiR-An**), the singlet excited state of **SiR-An** deactivates through the same pathway of that of SiR monomer, but in a faster manner because of the increased rate of internal conversion (Fig. 7 and Table S1).

Furthermore, based on all experimental results about H- and J-aggregate of **SiR-An** in the excited state, we concluded that (1) exciton is generated both in H- and J- aggregates of **SiR-An**; (2) the lifetime of one-exciton in **SiR-An** J-aggregate is approximately in the range of 0.5–1.9 ns, but most of them are easily quenched by EEA; (3) the relative number of exciton is proportional to the excitation power, which originates from the efficient EEA process and subsequent generation of additional states only under a high density of excitation photons. Finally, we tentatively suggest the weak fluorescence of **SiR-An** J-aggregate is due to substantial EEA occurring in a short coherent J-aggregate ($n \approx 3$–4) that composes a large J-aggregate (a few hundred nm). The obtained experimental results also implicate that kinds of excited states and their fates the self-assembly and excitation conditions.

It is intriguing that the shape of the absorption spectra of **TMR-An** and **SiR-An** exciton in J-aggregate are similar to those of previously reported porphyrin and cyanine derivatives. Considering porphyrin and cyanine derivatives are famous building blocks in the natural light harvesting system and the artificial energy transport wire in practice, this resemblance in the excited state and high molecular ε of **SiR-An** J-aggregate in the NIR region (> 10^5 M^{-1} cm^{-1} at around 740 nm as shown in Fig. S3) indicates the potential of rhodamine derivatives in the similar applications. Additionally, the relative population of exciton in **SiR-An** J-aggregate rather increases as the excitation power becomes stronger, which makes **SiR-An** further appropriate because long exciton lifetime is related to more participation into the photochemical reaction in the photosynthetic system.

Finally, we strongly believe the dyad composed of rhodamine and anthracene moiety holds great potential because both moieties have been substantially investigated for various important light-related phenomena and applications: bioimaging, dye laser, and photosensitizer of photocatalyst for rhodamine; singlet fission, triplet-triplet annihilation, exciton/charge transfer, and photo-induced dimerization for anthracene. H- and J-aggregate formation of rhodamine and anthracene dyad implies that the listed phenomenon and applications above can be converged together through supramolecular structure, resulting in surprising properties. We are currently carrying out subsequent studies to develop rational design of rhodamine and anthracene dyads to control their photophysical properties.

Acknowledgements

We thank S. Tojo (Osaka University) for the pulse radiolysis measurements and A. Sugimoto and A. Kuroda (Osaka University) for the assistance of chemical synthesis. We also thank T. Tachikawa (Kobe University) for our fruitful discussions. This work was partly supported by the Innovative Project for Advanced Instruments, Renovation Center of Instruments for Science Education and Technology, Osaka University, and a Grant-in-Aid for Scientific Research (Projects 25220806, 25288035, and others) from the Ministry of Education, Culture, Sports, Science and Technology (MEXT) of the Japanese Government.

References

1 M. Fu, Y. Xiao, X. Qian, D. Zhao and Y. Xu, *Chem. Commun.*, 2008, 1780.
2 Y. Koide, Y. Urano, K. Hanaoka, T. Terai and T. Nagano, *ACS Chem. Biol.*, 2011, **6**, 600.
3 A. Gahlmann and W. E. Moerner, *Nat. Rev. Micro.*, 2014, **12**, 9.
4 N. Bag and T. Wohland, *Ann. Rev. Phys. Chem.*, 2014, **65**, 225.
5 A. M. Smith, M. C. Mancini and S. Nie, *Nat. Nanotechnol.*, 2009, **4**, 710.
6 J. E. Aubin, *J. Histochem. Cytochem.*, 1979, **27**, 36.
7 S. Kim, M. Fujitsuka, N. Tohnai, T. Tachikawa, I. Hisaki, M. Miyata and T. Majima, *Chem. Commun.*, 2015, **51**, 11580.
8 S. Kim, T. Tachikawa, M. Fujitsuka and T. Majima, *J. Am. Chem. Soc.*, 2014, **136**, 11707.
9 G. Lukinavičius, K. Umezawa, N. Olivier, A. Honigmann, G. Yang, T. Plass, V. Mueller, L. Reymond, I. R. Corrêa, Z. G. Luo, C. Schultz, E. A. Lemke, P. Heppenstall, C. Eggeling, S. Manley and K. Johnsson, *Nat. Chem.*, 2013, **5**, 132.
10 S.-N. Uno, M. Kamiya, T. Yoshihara, K. Sugawara, K. Okabe, M. C. Tarhan, H. Fujita, T. Funatsu, Y. Okada, S. Tobita and Y. Urano, *Nat. Chem.*, 2014, **6**, 681.
11 G. Lukinavicius, L. Reymond, E. D'Este, A. Masharina, F. Gottfert, H. Ta, A. Guther, M. Fournier, S. Rizzo, H. Waldmann, C. Blaukopf, C. Sommer, D. W. Gerlich, H.-D. Arndt, S. W. Hell and K. Johnsson, *Nat. Meth.*, 2014, **11**, 731.
12 Y. Kushida, T. Nagano and K. Hanaoka, *Analyst*, 2015, **140**, 685.
13 Y. Sagara, T. Komatsu, T. Ueno, K. Hanaoka, T. Kato and T. Nagano, *J. Am. Chem. Soc.*, 2014, **136**, 4273.
14 S.-J. Yoon, J. W. Chung, J. Gierschner, K. S. Kim, M.-G. Choi, D. Kim and S. Y. Park, *J. Am. Chem. Soc.*, 2010, **132**, 13675.
15 Y. Hong, J. W. Y. Lam and B. Z. Tang, *Chem. Soc. Rev.*, 2011, **40**, 5361.
16 Y.-D. Lee, C.-K. Lim, A. Singh, J. Koh, J. Kim, I. C. Kwon and S. Kim, *ACS Nano*, 2012, **6**, 6759.
17 Y. Shirasaki, S. Kamino, M. Tanioka, K. Watanabe, Y. Takeuchi, S. Komeda and S. Enomoto, *Chem.–Asian J.*, 2013, **8**, 2609.
18 S. Verma and H. N. Ghosh, *J. Phys. Chem. Lett.*, 2012, **3**, 1877.
19 M. M. Sartin, C. Huang, A. S. Marshall, N. Makarov, S. Barlow, S. R. Marder and J. W. Perry, *J. Phys. Chem. A*, 2013, **118**, 110.
20 M. Ogawa, N. Kosaka, P. L. Choyke and H. Kobayashi, *ACS Chem. Biol.*, 2009, **4**, 535.
21 V. Huber, M. Katterle, M. Lysetska and F. Würthner, *Angew. Chem. Int. Ed.*, 2005, **44**, 3147.
22 J. Seo, J. W. Chung, J. E. Kwon and S. Y. Park, *Chem. Sci.*, 2014, **5**, 4845.
23 M. Ferguson, P. Beaumont, S. Jones, S. Navaratnam and B. Parsons, *Phys. Chem. Chem. Phys.*, 1999, **1**, 261.
24 Y. Urano, M. Kamiya, K. Kanda, T. Ueno, K. Hirose and T. Nagano, *J. Am. Chem. Soc.*, 2005, **127**, 4888.
25 S. Kim, M. Fujitsuka and T. Majima, *J. Phys. Chem. B*, 2013, **117**, 13985.
26 T. Miura, Y. Urano, K. Tanaka, T. Nagano, K. Ohkubo and S. Fukuzumi, *J. Am. Chem. Soc.*, 2003, **125**, 8666.
27 S. Fukuzumi, K. Ohkubo and T. Okamoto, *J. Am. Chem. Soc.*, 2002, **124**, 14147.
28 B. Z. Packard, A. Komoriya, D. D. Toptygin and L. Brand, *J. Phys. Chem. B*, 1997, **101**, 5070.
29 C. Nasr, D. Liu, S. Hotchandani and P. V. Kamat, *J. Phys. Chem.*, 1996, **100**, 11054.
30 D. Setiawan, A. Kazaryan, M. A. Martoprawiro and M. Filatov, *Phys. Chem. Chem. Phys.*, 2010, **12**, 11238.
31 R. F. Fink, J. Seibt, V. Engel, M. Renz, M. Kaupp, S. Lochbrunner, H.-M. Zhao, J. Pfister, F. Würthner and B. Engels, *J. Am. Chem. Soc.*, 2008, **130**, 12858.
32 R. J. Lindquist, K. M. Lefler, K. E. Brown, S. M. Dyar, E. A. Margulies, R. M. Young and M. R. Wasielewski, *J. Am. Chem. Soc.*, 2014, **136**, 14912.
33 S. Choi, J. Bouffard and Y. Kim, *Chem. Sci.*, 2014, **5**, 751.
34 M. Kasha, H. R. Rawls and M. Ashraf El-Bayoumi, *Pure Appl. Chem.*, 1965, **11**, 371.
35 F. Sasaki and S. Kobayashi, *J. Lumin.*, 1997, **72–74**, 538-540.
36 K. Minoshima, M. Taiji, K. Misawa and T. Kobayashi, *Chem. Phys. Lett.*, 1994, **218**, 67.
37 E. Gaižauskas, S. Pakalnis and K. H. Feller, *Chem. Phys.*, 2001, **266**, 69.
38 A. E. Johnson, S. Kumazaki and K. Yoshihara, *Chem. Phys. Lett.*, 1993, **211**, 511.
39 O. A. Sytina, I. H. M. van Stokkum, R. van Grondelle and M. L. Groot, *J. Phys. Chem. A*, 2010, **115**, 3936.
40 I. V. Ryzhov, G. G. Kozlov, V. A. Malyshev and J. Knoester, *J. Chem. Phys.*, 2001, **114**, 5322.
41 E. Engel, K. Leo and M. Hoffmann, *Chem. Phys.*, 2006, **325**, 170.
42 C. Shahar, J. Baram, Y. Tidhar, H. Weissman, S. R. Cohen, I. Pinkas and B. Rybtchinski, *ACS Nano*, 2013, **7**, 3547.
43 S. F. Völker, A. Schmiedel, M. Holzapfel, K. Renziehausen, V. Engel and C. Lambert, *J. Phys. Chem. C*, 2014, **118**, 17467.
44 J. Larsen, B. Brüggemann, T. Polívka, V. Sundström, E. Åkesson, J. Sly and M. J. Crossley, *J. Phys. Chem. A*, 2005, **109**, 10654.
45 E. A. Margulies, L. E. Shoer, S. W. Eaton and M. R. Wasielewski, *Phys. Chem. Chem. Phys.*, 2014, **16**, 23735.

46 A. Schubert, V. Settels, W. Liu, F. Würthner, C. Meier, R. F. Fink, S. Schindlbeck, S. Lochbrunner, B. Engels and V. Engel, *J. Phys. Chem. Lett.*, 2013, **4**, 792.
47 E. H. A. Beckers, S. C. J. Meskers, A. P. H. J. Schenning, Z. Chen, F. Würthner, P. Marsal, D. Beljonne, J. Cornil and R. A. J. Janssen, *J. Am. Chem. Soc.*, 2005, **128**, 649.